

Spatial Non-Locality Induced Non-Markovian EIT in a Single Giant Atom

Y. T. Zhu  ^{1,2,3}, R. B. Wu ^{4,5}, and S. Xue  ^{1,2,3*}

¹*Department of Automation, Shanghai Jiao Tong University, Shanghai 200240, P. R. China*

²*Key Laboratory of System Control and Information Processing,
Ministry of Education of China, Shanghai 200240, P. R. China*

³*Shanghai Engineering Research Center of Intelligent Control and Management, Shanghai 200240, P. R. China*

⁴*Department of Automation, Tsinghua University, Beijing 100084, P. R. China and*

⁵*Beijing National Research Center for Information Science and Technology, Beijing 100084, P. R. China*

(Dated: March 11, 2022)

Giant atoms have exhibited counterintuitive but interesting phenomena such as non-exponential decays which would benefit quantum information processing. However, recent experiments on electromagnetically induced transparency (EIT) of giant atoms observed standard spectra only. In this letter, we present a full quantum model for observing EIT in a single giant atom rather than a semi-classical one in recent works. With this model and a quantum transport theory in real space, a class of non-Markovian EIT can be observed which has not been witnessed before. This new phenomenon results from spatial non-locality of a multiple distant coupling structure in the giant atom, which physically forces propagating fields between the coupling points behaving as standing waves. We also show that the spatial non-locality induced non-Markovianity can be represented by a time-delayed master equation where widely-used Born approximation in the existing works breaks down.

Introduction— Light-matter interaction lies in the core of quantum optics, and has been extended to microwave and acoustic domains with the help of superconducting quantum circuits and nano-acoustic elements, where we can investigate photon-phonon quantum coherence at single-quanta level [1–8]. In superconducting circuits, artificial atoms can be piezoelectrically coupled to acoustic waves at several distant points [7, 8], or electrically coupled to microwaves via multiple capacitors [9]. These artificial atoms with either structures refer to *giant atoms* [10].

Unlike small atoms, giant atoms possess some special features. The excitation spectra of a single giant atom can exhibit unconventional Lamb shifts and decay rates depending on the atomic transition frequency [1, 11]. This frequency-dependent property induces a non-exponential decay of atomic excitations [8, 12]. Also, atomic excitations can counterintuitively oscillate without decay when the number of coupling points is greater than two [13]. In addition, several giant atoms with proper arrangements can couple to each other via virtual photons although their decoherence to the shared waveguide is completely suppressed [9, 14].

Although these groundbreaking works preliminarily discover the special features of two-level giant atoms, only conventional results are shown in recent experiments on three-level giant atoms. For instance, only standard electromagnetically induced transparency (EIT) [15–17] was observed in a ladder-type giant atom with either acoustic couplings [18] or microwave couplings [19]. This reason would be that there is only one single-point acoustic coupling [18], or two coupling points are too close such that the time delay between them is extremely short [19]. Hence, whether it is possible to discover EIT with special features for a three-level giant atom is still an open

problem.

In this letter, we consider a Λ -type giant atom for observing EIT. We model this system in a full quantum way which is different from the semi-classical model in recent works[18, 19]. To exactly calculate the transmission spectrum of a probing field, we utilize a quantum transport theory in real space with which we discover unconventional EIT phenomenon. Also, we find the undesired spontaneous emission can be eliminated rather than suppressed by engineering the multiple-point-coupling structure such that the Λ -type configuration can be obtained from a Δ -type artificial atom. In addition, we show that the propagating waves inside the outermost coupling points behave as standing waves due to interference between bidirectional propagating modes. These results imply that the distant couplings induce spatial non-localities such that the dynamics of the giant atom obey a time-delayed non-Markovian master equation.

Model— We consider a Δ -type giant atom with levels $|1\rangle$, $|2\rangle$, and $|3\rangle$, and the corresponding transition frequencies ω_{21} , ω_{31} and ω_{32} . Here, the energy of the ground state $|1\rangle$ is assumed to be zero as a reference. The transitions $|3\rangle \leftrightarrow |1\rangle$ and $|2\rangle \leftrightarrow |1\rangle$ are respectively side coupled to waveguides A and B at multiple points x_n and \tilde{x}_m with indices $n = 1, 2, \dots, N$, $m = 1, 2$, and distances d, \tilde{d} , as shown in Fig. 1. The coupling strengths at these points are denoted as $g_{31}(x_n) = g_{31}e^{i\alpha x_n}$, $g_{21}(\tilde{x}_m) = g_{21}e^{i\beta \tilde{x}_m}$ with wavevectors α and β for modes in the waveguide A and B , respectively. Here, we take the waveguide A as a channel of a probe field for observing its transmission and the waveguide B as a reservoir leading to the spontaneous emission in the transition $|2\rangle \leftrightarrow |1\rangle$. Here, we consider the modes in both waveguides are photons, but the following results can be applied to phonons when the atom couples to surface acoustic waves via multiple

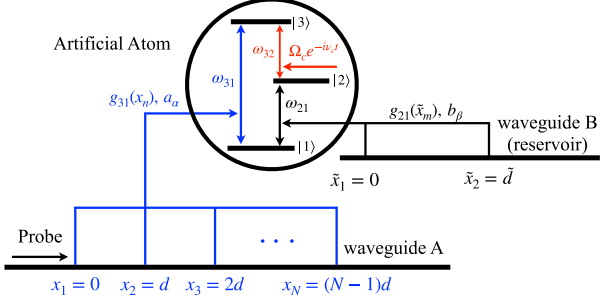


FIG. 1. Schematic of a Δ -type giant atom. The transition $|1\rangle \leftrightarrow |3(2)\rangle$ is coupled to the waveguide A (B) via multiple coupling points with an equal distance $d(\tilde{d})$. $g_{31}(x_n)$ and $g_{21}(\tilde{x}_m)$ denote the position-dependent coupling strength. Here, the waveguide B is taken as a reservoir resulting in the undesired spontaneous emission of the atom, while we take the waveguide A as a channel of a probe field. A classical driving with an angular frequency ν_c and a Rabi frequency Ω_c is applied to the transition $|2\rangle \leftrightarrow |3\rangle$ to induce EIT.

interdigital transducers. To induce EIT phenomenon, a classical driving field with an angular frequency ν_c and a Rabi frequency Ω_c is applied to the transition $|2\rangle \leftrightarrow |3\rangle$.

Different from the recent works [18, 19], the probe field herein is quantized. Under rotating wave approximation at the frequency ν_c , an effective Hamiltonian of the system in real space reads

$$\begin{aligned}
H_{\text{eff}} = & (\omega_{21} + \nu_c - \frac{i\gamma_2}{2})|2\rangle\langle 2| + (\omega_{31} - \frac{i\gamma_3}{2})|3\rangle\langle 3| + \\
& (\Omega_c|3\rangle\langle 2| + H.c.) - \sum_{D=L,R} f_D \int dx a_D^\dagger(x) (iv_g \frac{\partial}{\partial x}) a_D(x) + \\
& \sum_{D=L,R} \int dx b_D^\dagger(x) (\nu_c - i f_D \tilde{v}_g \frac{\partial}{\partial x}) b_D(x) + \\
& \tilde{g}_{31} \sum_{D=L,R} \sum_{n=1}^N \int dx \delta(x - x_n) (|3\rangle\langle 1| a_D(x) + H.c.) + \\
& \tilde{g}_{21} \sum_{D=L,R} \sum_{m=1}^2 \int dx \delta(x - \tilde{x}_m) (|2\rangle\langle 1| b_D(x) + H.c.), \quad (1)
\end{aligned}$$

where we set $\hbar = 1$, $f_R = 1$, $f_L = -1$, and the group velocity of the field in the waveguide A (B) is v_g (\tilde{v}_g). The bosonic annihilation operators a and b with subscripts R and L are for the right- and left-going modes, respectively. The damping rates γ_2 and γ_3 are introduced to describe non-waveguide losses of the atom [20]. The Dirac δ function $\delta(x - x_n(\tilde{x}_m))$ indicates interacting positions. For simplicity, we have assumed that the coupling strengths at each coupling point are identical and denoted as $\tilde{g}_{3(2)1}$, and linear dispersion relations hold in both waveguides. See Refs. [20, 21] for more details of derivation.

Single-photon scattering— To investigate EIT at a single photon level, we assume that both the waveguides

and the atom are initially prepared in their ground states $|\text{vac}\rangle$ and $|1\rangle$. A single photon is incident from x_1 to x_N and thus its scattering eigenstate $|\Psi\rangle$ in single-excitation subspace [22, 23] is written as

$$\begin{aligned}
|\Psi\rangle = & \int dx \left[\phi_R^\alpha(x) a_R^\dagger(x) + \phi_L^\alpha(x) a_L^\dagger(x) \right] |\text{vac}, 1\rangle + \\
& \int dx \left[\phi_R^\beta(x) b_R^\dagger(x) + \phi_L^\beta(x) b_L^\dagger(x) \right] |\text{vac}, 1\rangle + \\
& e_2 |\text{vac}, 2\rangle + e_3 |\text{vac}, 3\rangle, \quad (2)
\end{aligned}$$

where $e_{2(3)}$ is the atomic excitation amplitude of the state $|2(3)\rangle$. According to the interaction terms in the last two lines of Eq. (1), we plot Fig. 2 to describe the scattering process with ansatz. The atom at each coupling point acts as an individual δ -potential and thus the scattering process can be equivalently treated as that in a series of cascaded small atoms, which is analogous to those in Ref. [11, 24]. Therefore, the probability amplitude $\phi_{L(R)}^{\alpha(\beta)}(x)$ can be formally written as

$$\begin{aligned}
\phi_R^\alpha(x) = & e^{i\alpha x} [\theta(-x) + t_1 \theta(x) \theta(d-x) + \\
& t_2 \theta(x-d) \theta(2d-x) + \dots + t_{N-1} \theta(x-d) \dots \times \\
& \theta(x-(N-2)d) \theta((N-1)d-x) + t_N \theta(x-(N-1)d)], \\
\phi_L^\alpha(x) = & e^{-i\alpha x} [r_1 \theta(-x) + r_2 \theta(x) \theta(d-x) + \dots + \\
& r_N \theta(x) \theta(x-d) \dots \theta(x-(N-2)d) \theta((N-1)d-x)], \quad (3) \\
\phi_R^\beta(x) = & e^{i\beta x} [\tilde{t}_1 \theta(x) \theta(\tilde{d}-x) + \tilde{t}_2 \theta(x) \theta(x-\tilde{d})], \\
\phi_L^\beta(x) = & e^{-i\beta x} [\tilde{r}_1 \theta(-x) + \tilde{r}_2 \theta(x) \theta(\tilde{d}-x)],
\end{aligned}$$

where the Heaviside step function $\theta(x)$ is used to distinguish different scattering intervals. For the waveguide A , the transmission and reflection amplitudes in the corresponding intervals are denoted as t_1, t_2, \dots, t_n and r_1, r_2, \dots, r_n , respectively. Similarly, \tilde{t}_1, \tilde{t}_2 and \tilde{r}_1, \tilde{r}_2 denote those in the waveguide B . Noted that in Eq. (3) we only take the single transmission and reflection inside two neighboring points into account and ignore high-order scattering processes.

Substituting Eqs. (1)-(3) into the stationary Shrödinger equation $H_{\text{eff}}|\Psi\rangle = \omega|\Psi\rangle$, we obtain the transmission amplitude of the probe field

$$t_N = \frac{(\Delta_F + i\gamma)(\Delta_S + \frac{i\gamma_3}{2}) - |\Omega_c|^2}{(\Delta_F + i\gamma)(\Delta_S + \frac{i\gamma_3}{2} + i\Gamma_{31}^{(N)}) - |\Omega_c|^2} \quad (4)$$

and the excitation of the atom

$$e_3 = \frac{(\Delta_F + i\gamma)\tilde{g}_{31} \sum_{n=1}^N e^{(N-n)i(\Delta_{31} + \omega_3)\tau}}{(\Delta_F + i\gamma)(\Delta_S + \frac{i\gamma_3}{2} + i\Gamma_{31}^{(N)}) - |\Omega_c|^2} \quad (5)$$

with $\Delta_F = \Delta_{31} - \Delta_{32} - \Delta_r$, $\gamma = \frac{i\gamma_2}{2} + i\Gamma_{21}$, $\Delta_S = \Delta_{31} - \Delta_L^{(N)}$, the detunings $\Delta_{31} = \omega - \omega_{31}$ and $\Delta_{32} = \nu_c - (\omega_{31} - \omega_{21})$, and the eigenfrequency of the incoming photon $\omega = v_g\alpha$. Both of them are affected by the frequency shift

$$\Delta_r = \Gamma_{21} \sin(\omega\tilde{\tau}) \quad (6)$$

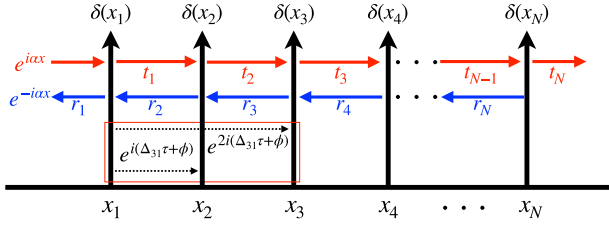


FIG. 2. Schematic of the scattering for the probe field. In real space, the giant atom behaves as a δ potential at each coupling point, which is similar to a series of cascaded small atoms. The joint transmission amplitudes t_1, t_2, \dots, t_{N-1} and reflection amplitudes r_2, r_3, \dots, r_N describe the single transmission and reflection between the neighboring two points, where the transmission amplitude t_N and reflection amplitude r_1 contain all the accumulated phases. An example of the accumulated phase for the right-forward propagating process is given in the red box.

and the effective decay rate

$$\Gamma_{21}^r = \Gamma_{21} (1 + \cos(\omega_\beta \tilde{\tau})) \quad (7)$$

where $\tilde{\tau} = \tilde{d}/\tilde{v}_g$ is a time delay and $\Gamma_{21} = 2\tilde{g}_{21}^2/\tilde{v}_g$. These two terms are induced by the waveguide B so that they depend on the parameters therein. Importantly, the decay rate Γ_{21}^r can be zero when $\omega_\beta \tilde{\tau} = (2k + 1)\pi, k = 0, 1, 2, \dots$. This means the bottom spontaneous emission in the Δ configuration can be totally eliminated, if we properly engineer the time delay $\tilde{\tau}$ with respect to a reservoir frequency ω_β . Hereafter, we assume that this condition is satisfied. In this way, we transform a Δ -type atom to a Λ -type one.

In addition, the couplings to the waveguide A induce the frequency-dependent Lamb shift

$$\Delta_L^{(N)} = \Gamma_{31} \sum_{n=1}^N (N - n) \sin(n\Delta_{31}\tau + n\phi) \quad (8)$$

and the modified decay rate

$$\Gamma_{31}^{(N)} = \Gamma_{31} \sum_{n=1}^N \left(\frac{N}{2} + (N - n) \cos(n\Delta_{31}\tau + n\phi) \right) \quad (9)$$

with $\Gamma_{31} = 2\tilde{g}_{31}^2/v_g$, $\tau = d/v_g$, and $\phi = \omega_{31}\tau$. The first term in the addend of Eq. (9) denotes the joint decay rates attributed by the N individual coupling points, while the second term is led by the spatial non-local couplings.

Note that the transmission amplitude t_N (4) is modified by Eqs. (8) and (9) with sinusoidal components, which indicates that the transmission spectra would be different from those in traditional EIT. Particularly, when $N = 1$, the second term vanishes such that the decay rate $\Gamma_{31}^{(N)}$ reduces to a constant $\Gamma_{31}/2$; i.e., the giant atom reduces to a small atom, which is consistent with that in Refs. [20, 25].

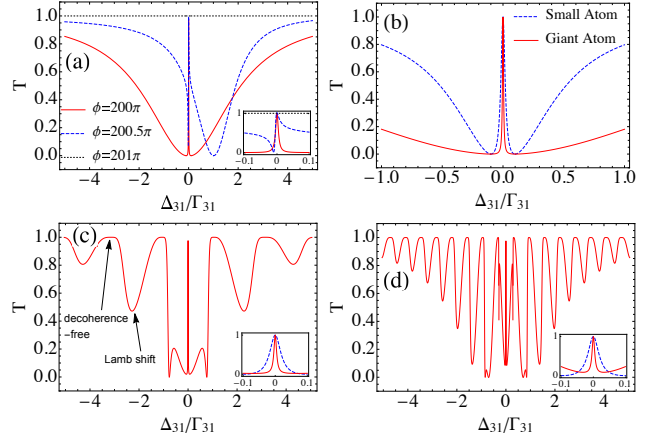


FIG. 3. Transmission spectra of the giant atom in the EIT regime with $N = 2$ and $\Omega_c = 0.1\Gamma_{31}$. (a) With a small $\tau = 0.05/\Gamma_{31}$, the spectra have only one peak since where both the Lamb shift $\Delta_{31}^{(2)}$ and decay rate $\Gamma_{31}^{(2)}$ are mainly determined by the phase ϕ . (b) Compared to small atoms, the transparent window $\Gamma_w \simeq |\Omega_c|^2/\Gamma_{31}^{(2)}$ is clearly modified by the phase ϕ , where $\phi = 200\pi, \tau = 0.05/\Gamma_{31}$. In (c) $\tau = 3/\Gamma_{31}$ and (d) $\tau = 10/\Gamma_{31}$, we show the unconventional EIT spectra with increased time delays τ for a fixed phase $\phi = 200\pi$. In both cases, $\Delta_{31}\tau$ dominate the variations of $\Delta_{31}^{(2)}$ and $\Gamma_{31}^{(2)}$ such that absorption peaks (arrow to Lamb shift) and transparent subpeaks (arrow to decoherence free) appear alternately. The blue dashed lines in insets represent the small atom case. Other parameters are: $\Delta_{32} = \gamma_2 = \gamma_3 = 0$.

Unconventional EIT— With the above results, we then find the following unconventional EIT phenomena. We set $N = 2$ and define the transmission coefficient as $T = |t_2|^2$. The time delay $\tau = \{0.05, 3, 10\}/\Gamma_{31}$ is set to cover those in both the microwave-coupling and acoustic-coupling regimes in Refs. [8, 19].

In the EIT regime, we plot the transmission spectra T in Fig. 3. When the time delay $\tau = 0.05/\Gamma_{31}$ is small enough and $\Delta_{31} \ll \omega_{31}$, the Lamb shift $\Delta_L^{(2)}$ and the decay rate $\Gamma_{31}^{(2)}$ are mainly determined by the phase ϕ such that the spectrum has a single absorption peak determined by the frequency ω_{31} as shown in Fig. 3(a), which is consistent with that in Ref. [11]. Particularly, when $\phi = (2k + 1)\pi$, we have $\Delta_L^{(2)} = \Gamma_{31}^{(2)} = 0$ where the system is decoherence-free; i.e., the giant atom is totally decoupled from the waveguide A , although there still exists a non-zero coupling Γ_{31} . This is represented by the black dot line in Fig. 3(a). Further, with a given phase $\phi = 200\pi$, we increase the time delay τ so that decoherence-free bands and Lamb-shift-induced absorption peaks appear alternatively and become dense, as shown in Figs. 3(b)-(d). This is because the absorption peaks with a modified linewidth $\Gamma_{31}^{(2)}$ appear in the single-photon resonance $\Delta_{31} = \Delta_L^{(2)}$ (see Δ_S in Eq. (4)). In addition, since the induced transparency occurs at two-photon resonance $\Delta_{31} - \Delta_{32} = 0$ (see Δ_F in Eq. (4)),

the transparency window $\Gamma_w \simeq |\Omega_c|^2/\Gamma_{31}^{(2)}$ is only modified by the decay rate $\Gamma_{31}^{(2)}$ which depends on the initial phase ϕ , as shown in Fig. 3(b) and the insets in Figs. 3(c)-(d).

Note that by increasing the Rabi frequency Ω_c , similar solutions can also be found in the Autler-Townes Splitting (ATS) regime [26], as shown in Ref. [21]. Besides, a stronger modification can be obtained by increasing the number of the coupling points. For instance, the maximum value of $\Gamma_{31}^{(3)} = 2\Gamma_{31} \left[\frac{1}{2} + \cos(\Delta_{31}\tau + \phi) \right]^2$ is greatly enhanced compared to $\Gamma_{31}^{(2)} = 2\Gamma_{31} \cos^2 \left(\frac{\Delta_{31}\tau + \phi}{2} \right)$. See Ref. [21] for more details.

Standing-wave explanation— The unconventional EIT in the giant atom exhibit multiple-peak spectra which are similar to those in Ref. [12]. They mathematically attribute the multiple peaks to the multi-value property of a complex Lambert W function. However, since the frequency of input single photons corresponds to the eigenenergy of the system, it should be real rather than complex without \mathcal{PT} -symmetry breaking [27–29]. Hence, physics behind the unconventional EIT should be uncovered.

From a perspective of coherent feedback [30], discrete modes in the feedback loop can result in multiple-peak excitations. In a similar way, since Eqs. (8)-(9) take a sinusoidal form, we guess it resulting from a boundary condition of standing waves, following which we consider that the giant atom acts as mirrors cutting the entire waveguide into several *cascaded cavities*. For a right-forward propagating field, it accumulates a phase $e^{ni(\Delta_{31}\tau + \phi)}$ when it passes through a cavity formed by two coupling points. Correspondingly, it accumulates a conjugate phase $e^{-ni(\Delta_{31}\tau + \phi)}$ during the propagation in an opposite direction. For instance, the photon accumulates a phase $e^{i(\Delta_{31}\tau + \phi)}$ from x_1 to x_2 , and thus from x_1 to x_3 it accumulates $2e^{i(\Delta_{31}\tau + \phi)}$ and $e^{2i(\Delta_{31}\tau + \phi)}$, etc., as shown in the red box of Fig. 2. Therefore, the interference between bidirectional propagating waves inside each cavity attributes to the sinusoidal form such that the standing waves therein lead the multiple peaks in Fig. 3.

The above standing-wave supposition can be verified by the joint transmission and reflection spectra, as shown in Fig. 4 where $\tilde{T} = |t_1|^2$ and $\tilde{R} = |r_2|^2$. As mentioned before, the standing wave comes from the interference between bidirectional modes and thus it requires a non-zero \tilde{T} and \tilde{R} . In addition, the normalization property of wave functions requires $\tilde{T} + \tilde{R} = 1$ in principle. Therefore, those unnormalized points should be attributed to the interference between the single transmission and reflection therein, since higher-order processes have been omitted in Eq. (3).

Time-delayed master equation— We further find interference-induced standing waves are a non-Markovian effect, where the dynamics of the giant atom obey a time-

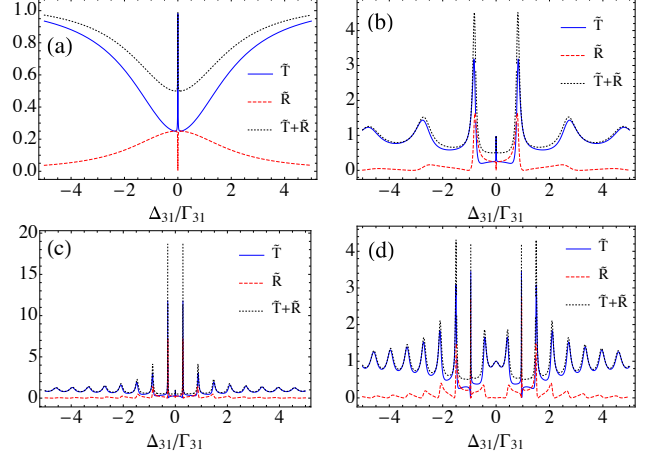


FIG. 4. Joint transmission and reflection spectra (a)-(c) in EIT regime with $\Omega_c = 0.1\Gamma_{31}$, and (d) in ATS regime with $\Omega_c = \Gamma_{31}$. $\tilde{T} + \tilde{R}$ (black dashed lines) is not always normalized except for two photon resonance. These non-normalized points indicates the interference between two directional modes. Parameters in plotting are: $\gamma_2 = \gamma_3 = \Delta_{32} = 0$, $\phi = 200\pi$, and in (a) $\tau = 0.05/\Gamma_{31}$; in (b) $\tau = 3/\Gamma_{31}$; in (c) and (d) $\tau = 10/\Gamma_{31}$.

delayed master equation

$$\begin{aligned} \dot{\rho}_a(t) = & -i[V_c(t), \rho_a(t)] + \gamma_{loc}\tilde{\mathcal{L}}_{loc}(t) + 2\Gamma'_{31}\tilde{\mathcal{L}}_{31}(t-n\tau) \\ & + 2\Gamma'_{21}\tilde{\mathcal{L}}_{21}(t-\tilde{\tau}) - i\Delta'_L[\sigma_{33}, \rho_a(t-n\tau)] \\ & - i\Delta'_r[\sigma_{22}, \rho_a(t-\tilde{\tau})], \end{aligned} \quad (10)$$

where $\rho_a(t)$ denotes the atomic density operator, $V_c(t) = \sum_{n=1}^N (\Omega_p e^{-i\Delta_{31}t+i\alpha x_n} \sigma_{31} + H.c.) + (\Omega_c e^{-i\Delta_{31}t} \sigma_{32} + H.c.)$ is the interaction Hamiltonian with a weak probe field Ω_p , and $\sigma_{ij} = |i\rangle\langle j|$ with $i, j = 1, 2, 3$. The joint Lindblad term $\gamma_{loc}\tilde{\mathcal{L}}_{loc}(t) = (\gamma_{31} + N\Gamma_{31})\mathcal{L}[\sigma_{13}\rho_a(t)] + \gamma_{32}\mathcal{L}[\sigma_{23}\rho_a(t)] + \gamma_2^\phi\mathcal{L}[\sigma_{22}\rho_a(t)] + \gamma_3^\phi\mathcal{L}[\sigma_{33}\rho_a(t)] + \Gamma_{21}M\mathcal{L}[\sigma_{12}\rho_a(t)]$ denotes the time-localized loss with the non-waveguide decay $\gamma_{31(2)}$ and the pure dephasing rate $\gamma_{2(3)}^\phi$, where $\mathcal{L}[O\rho_a(t)]$ is the standard Lindblad superoperator for an arbitrary operator O . While the non-Markovian effect is shown in those remaining time-delayed terms, where $\Gamma'_{31} = \Gamma_{31} \sum_{n=1}^N (N-n) \cos(n\omega_{31}\tau)$, $\Delta'_L = \Gamma_{31} \sum_{n=1}^N (N-n) \sin(n\omega_{31}\tau)$, $\Gamma'_{21} = \Gamma_{21} \cos(\omega_{21}\tilde{\tau})$, $\Delta'_r = \Gamma_{21} \sin(\omega_{21}\tilde{\tau})$, $\tilde{\mathcal{L}}_{31}(t-n\tau) = \mathcal{L}[\sigma_{13}\rho_a(t-n\tau)]$, and $\tilde{\mathcal{L}}_{21}(t-\tilde{\tau}) = \mathcal{L}[\sigma_{12}\rho_a(t-\tilde{\tau})]$. In the steady states, the solution of density matrix element $\tilde{\rho}_{31}$ in Eq. (10) reads

$$\tilde{\rho}_{31} = \frac{(\Delta_F + i\gamma) \Omega_p \sum_{n=1}^N e^{(N-n)i(\Delta_{31}\tau + \phi)}}{(\Delta_F + i\gamma)(\Delta_S + \frac{i\gamma_3}{2} + i\Gamma_{31}^{(N)}) - |\Omega_c|^2}, \quad (11)$$

which is consistent with the excitation e_3 (5) under the replacement $\tilde{g}_{31} \rightarrow \Omega_p$. The consistency shows that the non-exponential decay in the time domain [8] and the multiple peaks in the frequency domain are two sides of a coin for the non-Markovian effects. Spatially, they reflect as the standing waves.

Unlike the common non-Markovian dynamics [31–33], the non-Markovian effect in giant atoms results from the spatial non-local couplings rather than the spectral property of interacting environments. Besides, it vanishes under Born approximation $\rho_a(t - n\tau), \rho_a(t - \tilde{\tau}) \rightarrow \rho_a(t)$ and thus the Lamb shift and modified decay rate reduce to depend on atomic frequencies as shown in Ref. [11]. However, this approximation is valid only when the time delays τ and $\tilde{\tau}$ are small enough compared to the time scale of relaxation $1/\Gamma_{31}$.

Conclusion— In conclusion, we have discovered non-Markovian EIT and ATS in a single giant atom, which is led by the spatial non-local couplings and physically corresponds to the standing waves. Our results predict that the unconventional EIT can be observed in an experiment when the time delay between two neighboring couplings should be comparable to the relaxation time $1/\Gamma_{31}$. Besides, we present a time-delayed master equation to describe this non-Markovian effect which breaks Born approximation down. This equation opens a possibility in designing filters and feedbacks [34–36]. Also, our method using multi-point couplings can eliminate the undesired transition instead of employing multiple Josephson junctions [37] or cavities [38–40], which promotes the development of on-chip quantum memories based on EIT protocol [41].

Acknowledgements— We thank W. Z. Jia, Q. Y. Cai, L. Du, and X. M. Jin for fruitful discussion. This work is supported by the National Natural Science Foundation of China (NSFC) under Grants 61873162, 61973317. This work was also supported by the Open Research Project of the State Key Laboratory of Industrial Control Technology, Zhejiang University, China (No. ICT2021B24).

* shbxue@sjtu.edu.cn

[1] M. V. Gustafsson, T. Aref, A. F. Kockum, M. K. Ekström, G. Johansson, and P. Delsing, Propagating phonons coupled to an artificial atom, *Science* **346**, 207 (2014).

[2] M. J. A. Schuetz, E. M. Kessler, G. Giedke, L. M. K. Vandersypen, M. D. Lukin, and J. I. Cirac, Universal quantum transducers based on surface acoustic waves, *Phys. Rev. X* **5**, 031031 (2015).

[3] Y. Chu, P. Kharel, W. H. Renninger, L. D. Burkhardt, L. Frunzio, P. T. Rakich, and R. J. Schoelkopf, Quantum acoustics with superconducting qubits, *Science* **358**, 199 (2017).

[4] Y. Chu, P. Kharel, T. Yoon, L. Frunzio, P. T. Rakich, and R. J. Schoelkopf, Creation and control of multi-phonon fock states in a bulk acoustic-wave resonator, *Nature* **563**, 666 (2018).

[5] K. J. Satzinger, Y. P. Zhong, H.-S. Chang, G. A. Peairs, A. Bienfait, M.-H. Chou, A. Y. Cleland, C. R. Conner, E. Dumur, J. Grebel, I. Gutierrez, B. H. November, R. G. Povey, S. J. Whiteley, D. D. Awschalom, D. I. Schuster, and A. N. Cleland, Quantum control of surface acoustic-wave phonons, *Nature* **563**, 661 (2018).

[6] M. K. Ekström, T. Aref, A. Ask, G. Andersson, B. Suri, H. Sanada, G. Johansson, and P. Delsing, Towards phonon routing: controlling propagating acoustic waves in the quantum regime, *New J. Phys.* **21**, 123013 (2019).

[7] R. Manenti, A. F. Kockum, A. Patterson, T. Behrle, J. Rahamim, G. Tancredi, F. Nori, and P. J. Leek, Circuit quantum acoustodynamics with surface acoustic waves, *Nat. Comm.* **8**, 975 (2017).

[8] G. Andersson, B. Suri, L. Guo, T. Aref, and P. Delsing, Non-exponential decay of a giant artificial atom, *Nat. Phys.* **15**, 1123 (2019).

[9] B. Kannan, M. J. Ruckriegel, D. L. Campbell, A. Frisk Kockum, J. Braumuller, D. K. Kim, M. Kjaergaard, P. Krantz, A. Melville, B. M. Niedzielski, A. Vesalainen, R. Winik, J. L. Yoder, F. Nori, T. P. Orlando, S. Gustavsson, and W. D. Oliver, Waveguide quantum electrodynamics with superconducting artificial giant atoms, *Nature* **583**, 775 (2020).

[10] A. Frisk Kockum, Quantum optics with giant atoms—the first five years, in *Mathematics for Industry* (Springer Singapore, 2020) p. 125–146.

[11] A. Frisk Kockum, P. Delsing, and G. Johansson, Designing frequency-dependent relaxation rates and lamb shifts for a giant artificial atom, *Phys. Rev. A* **90**, 013837 (2014).

[12] L. Guo, A. Grimsmo, A. F. Kockum, M. Pletyukhov, and G. Johansson, Giant acoustic atom: A single quantum system with a deterministic time delay, *Phys. Rev. A* **95**, 053821 (2017).

[13] L. Guo, A. F. Kockum, F. Marquardt, and G. Johansson, Oscillating bound states for a giant atom, *Phys. Rev. Research* **2**, 043014 (2020).

[14] A. F. Kockum, G. Johansson, and F. Nori, Decoherence-free interaction between giant atoms in waveguide quantum electrodynamics, *Phys. Rev. Lett.* **120**, 140404 (2018).

[15] S. E. Harris, J. E. Field, and A. Imamoglu, Nonlinear optical processes using electromagnetically induced transparency, *Phys. Rev. Lett.* **64**, 1107 (1990).

[16] K.-J. Boller, A. Imamoglu, and S. E. Harris, Observation of electromagnetically induced transparency, *Phys. Rev. Lett.* **66**, 2593 (1991).

[17] M. Fleischhauer, A. Imamoglu, and J. P. Marangos, Electromagnetically induced transparency: Optics in coherent media, *Rev. Mod. Phys.* **77**, 633 (2005).

[18] G. Andersson, M. K. Ekström, and P. Delsing, Electromagnetically induced acoustic transparency with a superconducting circuit, *Phys. Rev. Lett.* **124**, 240402 (2020).

[19] A. M. Vadiraj, A. Ask, T. G. McConkey, I. Nsanzineza, C. W. S. Chang, A. F. Kockum, and C. M. Wilson, Engineering the level structure of a giant artificial atom in waveguide quantum electrodynamics, *Phys. Rev. A* **103**, 023710 (2021).

[20] J.-T. Shen and S. Fan, Theory of single-photon transport in a single-mode waveguide. i. coupling to a cavity containing a two-level atom, *Phys. Rev. A* **79**, 023837 (2009).

[21] Supplement materials.

[22] W. Z. Jia, Y. W. Wang, and Y.-x. Liu, Efficient single-photon frequency conversion in the microwave domain using superconducting quantum circuits, *Phys. Rev. A* **96**, 053832 (2017).

[23] M. Bradford and J.-T. Shen, Single-photon frequency conversion by exploiting quantum interference, *Phys. Rev. A*

85, 043814 (2012).

[24] J. Gough and M. R. James, The series product and its application to quantum feedforward and feedback networks, *IEEE Trans. Autom. Control* **54**, 2530 (2009).

[25] Y. T. Zhu and W. Z. Jia, Single-photon quantum router in the microwave regime utilizing double superconducting resonators with tunable coupling, *Phys. Rev. A* **99**, 063815 (2019).

[26] S. H. Autler and C. H. Townes, Stark effect in rapidly varying fields, *Phys. Rev.* **100**, 703 (1955).

[27] C. M. Bender and S. Boettcher, Real spectra in non-hermitian hamiltonians having \mathcal{PT} symmetry, *Phys. Rev. Lett.* **80**, 5243 (1998).

[28] B. Peng, S. K. Özdemir, F. Lei, F. Monifi, M. Gianfreda, G. L. Long, S. Fan, F. Nori, C. M. Bender, and L. Yang, Parity-time-symmetric whispering-gallery microcavities, *Nat. Phys.* **10**, 394 (2014).

[29] L. Chang, X. Jiang, S. Hua, C. Yang, J. Wen, L. Jiang, G. Li, G. Wang, and M. Xiao, Parity-time symmetry and variable optical isolation in active-passive-coupled microresonators, *Nat. Photonics* **8**, 524 (2014).

[30] N. Német, A. Carmele, S. Parkins, and A. Knorr, Comparison between continuous- and discrete-mode coherent feedback for the jaynes-cummings model, *Phys. Rev. A* **100**, 023805 (2019).

[31] H.-P. Breuer, E.-M. Laine, J. Piilo, and B. Vacchini, Colloquium: Non-Markovian dynamics in open quantum systems, *Rev. Mod. Phys.* **88**, 021002 (2016).

[32] S.-B. Xue, R.-B. Wu, W.-M. Zhang, J. Zhang, C.-W. Li, and T.-J. Tarn, Decoherence suppression via non-markovian coherent feedback control, *Phys. Rev. A* **86**, 052304 (2012).

[33] W.-M. Zhang, P.-Y. Lo, H.-N. Xiong, M. W.-Y. Tu, and F. Nori, General non-markovian dynamics of open quantum systems, *Phys. Rev. Lett.* **109**, 170402 (2012).

[34] S. Xue, R. Wu, M. R. Hush, and T.-J. Tarn, Non-Markovian coherent feedback control of quantum dot systems, *Quantum Sci. Technol.* **2**, 014002 (2017).

[35] S. Xue, M. R. Hush, and I. R. Petersen, Feedback tracking control of non-markovian quantum systems, *IEEE Trans. Control Syst. Technol.* **25**, 1552 (2017).

[36] S. Xue, T. Nguyen, M. R. James, A. Shabani, V. Ugrinovskii, and I. R. Petersen, Modeling for non-markovian quantum systems, *IEEE Trans. Control Syst. Technol.* **28**, 2564 (2020).

[37] V. E. Manucharyan, J. Koch, L. I. Glazman, and M. H. Devoret, Fluxonium: Single cooper-pair circuit free of charge offsets, *Science* **326**, 113 (2009).

[38] A. A. Abdumalikov, O. Astafiev, A. M. Zagoskin, Y. A. Pashkin, Y. Nakamura, and J. S. Tsai, Electromagnetically induced transparency on a single artificial atom, *Phys. Rev. Lett.* **104**, 193601 (2010).

[39] S. Novikov, T. Sweeney, J. E. Robinson, S. P. Premaratne, B. Suri, F. C. Wellstood, and B. S. Palmer, Raman coherence in a circuit quantum electrodynamics lambda system, *Nat. Phys.* **12**, 75 (2016).

[40] J. Long, H. S. Ku, X. Wu, X. Gu, R. E. Lake, M. Bal, Y.-x. Liu, and D. P. Pappas, Electromagnetically induced transparency in circuit quantum electrodynamics with nested polariton states, *Phys. Rev. Lett.* **120**, 083602 (2018).

[41] M. Afzelius, N. Gisin, and H. Riedmatten, Quantum memory for photons, *Phys. Today* **68**, 42 (2015).